Euronoise 2018 Crete

Acoustic Source Localization in Hemispherical Harmonics Domain

Deepika Kumari
Department of EE, Indian Institute of Technology, Delhi.

Lalan Kumar
Department of EE & Bharti School of Telecommunication, Indian Institute of Technology, Delhi

Summary
This paper addresses the issue of far-field sound source localization using hemispherical microphone array (HMA). Rather than conventional spherical harmonics (SH), hemispherical harmonics (HSH) basis functions are utilized herein. The hemispherical harmonics basis functions provide more accurate representation of hemispherical functions when compared to spherical harmonics. Source localization using spherical microphone array makes use of spherical harmonics. Previous work presented sound capture and beamforming using HMA that is based on acoustic image principal in spherical harmonics domain. However, hemispherical harmonics has hitherto not been investigated for source localization. Optimal array processing methods such as MUltiple SIgnal Classification (MUSIC) and minimum variance distortionless response (MVDR) are reformulated in HSH domain. Hemispherical harmonics MUSIC (HSH-MUSIC) and hemispherical harmonics MVDR (HSH-MVDR) methods are presented for source localization. The relative performance is presented using various experiments on source localization.

PACS no. 43.60.Jn

1. Introduction

Acoustic source localization in spherical harmonics (SH) domain has been an active area of research [1]-[5]. A spherical microphone array (SMA) is utlized to acquire the signal. The increasing use of SMA for source localization and beamforming is because of the ease of array processing in SH domain with no spatial ambiguity [6]. The SH domain processing additionaly offers dimensionality reduction for computational efficiency [7]. Various far-field and near-field source localization algorithms have been proposed in SH domain. Multiple SIgnal Classification (MUSIC) [8] is formulated in SH domain called SH-MUSIC in [9] . Spherical harmonics minimum variance distortionless response (SH-MVDR) is implemented in [7]. Estimation of signal parameters via rotational invariance techniques [10] algorithm is extended for spherical array in [11, 12]. An additional search free algorithm, SH-root-MUSIC for source localization using SMA is proposed in [13]. SH data model for near field source is developed in [3].

Building of spherical microphone array over a rigid sphere is a challenging task. Additionally, utilization of entire sphere comes at the expence of more number of microphones and signals to process. It is also uneconomic when the sources are present in restricted region of environment. A hemispherical microphone array (HMA) is utilized in [14] for sound acquisition and beamforming with sources placed on one side of a rigid plane. As the data is present only on half of the sphere, acoustic image principle is utilized herein to represent pressure using spherical harmonics. The proposed configuration and the principle is applicable only when a rigid plane is attached to the bottom of hemispherical array resulting in limited applications. This also add to complexity as it utilizes imaginary microphones and sources. It also requires to maintain uniformity and symmetry across the boundary of real and imaginary hemisphere. Spherical harmonics basis functions have been utilized in [15, 16, 17] to represent hemispherical functions that include bi-directional reflectance distribution function(BRDF) and incident radiance functions. However, spherical harmonics in general, are utilized to represent function defined over entire sphere. Accurate representation of data over hemisphere by SH requires more number of SH coefficients due to discontinuties at the boundary of the hemisphere [18]. A novel hemispherical harmonics (HSH) basis functions are proposed in [18] for representation of BRDF and hemispherical radiance

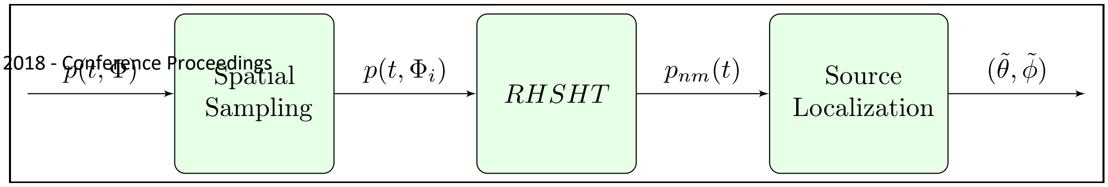

Figure 1: The processing framework for source localization using real hemispherical harmonics transform. The sound field is sampled using I microphones with i^{th} microphone placed at (r,Φ_i).

function. In this paper, the source localization is performed using hemispherical microphone array. Hence, the data is available only over hemisphere. For accurate representation of sound pressure over hemisphere, HSH basis functions are utilized. The real spherical harmonics basis functions are introduced first followed by the real HSH basis functions. A data model is derived in HSH domain. Far-field source localization is subsequently performed using HSH-MUSIC and HSH-MVDR.

2. The HSH Domain Data Model

We consider a HMA with I identical and omnidirectional microphones, placed on a hemisphere of radius r. The hemisphere could be wall mounted or table mounted. The HMA can also be formed by placing the microphones only over the upper half of the rigid spherical surface to save cost and computation. The angular position of the i^{th} microphone is denoted by $\Phi_i = (\theta_i,\phi_i)$, where θ_i is elevation angle, measured downward from positive z axis, and ϕ_i is the azimuth angle measured anticlockwise from positive x axis for the ith microphone. A sound field of L plane waves is incident on the array with wavenumber k. The direction of arrival of the l^{th} source is denoted by $\Psi_l = (\theta_l,\phi_l)$.

2.1. The Real SH Transform

The complete block diagram for hemispherical harmonics domain processing for source localization is illustrated in Figure 1. The localization is performed using discrete time domain acoustic signals $p(t)$, where t is the snapshot index. As $p(t)$ is real, *real* spherical harmonics transform (SHT) is applied. The associated processing has lower computational complexity when compared to complex SHT [21, p. 28]. The real SHT of a discrete time domain signal is given as [21]

$$p_{nm}(t) = \int_{\Phi\epsilon S^2} p(t,\Phi)[R_n^m(\Phi)]d\Phi, \qquad (1)$$

where $R_n^m(\Phi)$ is real valued spherical harmonics of order n and degree m given by

$$R_n^m(\theta,\phi) = \begin{cases} (-1)^{|m|}\sqrt{2}K_n^m \sin(|m|\phi)P_n^{|m|}(\cos\theta) & : m<0 \\ (-1)^{|m|}\sqrt{2}K_n^m \cos(m\phi)P_n^{m}(\cos\theta) & : m>0 \\ K_n^0 P_n^0(\cos\theta) & : m=0 \end{cases} \qquad (2)$$

The order n takes value from $[0,\infty)$ while m varies from $[-n,n]$, $|.|$ denotes the absolute value of $(.)$, K_n^m is the normalization value given by

$$K_n^m = \sqrt{\frac{(2n+1)(n-\mid m\mid)!}{4\pi(n+\mid m\mid)!}}. \qquad (3)$$

$P_n^m(\cos\theta)$ is the associated Legendre polynomials (ALPs) given by the relation

$$P_n^m(x) = \begin{cases} (-1)^m(1-x^2)^{m/2}\dfrac{d^m}{dx^m}P_n(x) & : m\geq 0 \\ (-1)^m\dfrac{(n-m)!}{(n+m)!}P_n^{|m|}(x) & : m<0 \end{cases} \qquad (4)$$

where $\cos\theta$ is replaced by x for simplicity. $P_n(x)$ is unassociated Legendre polynomials expressed as

$$P_n(x) = \frac{1}{2^n n!}\frac{d^n}{dx^n}(x^2-1)^n. \qquad (5)$$

The associated Legendre polynomials for different order n and same degree m are orthogonal over [-1,1] with weighting function as 1 [18]. The orthogonality relation is given by

$$\int_{-1}^{1} P_n^m(x)P_{n'}^m(x)dx = \frac{2\,(n+m)!}{(2n+1)\,(n-m)!}\delta_{nn'}. \qquad (6)$$

The inverse real SHT is given by

$$p(t,\Phi) = \sum_{n=0}^{\infty}\sum_{m=-n}^{n} p_{nm}(t)R_n^m(\Phi). \qquad (7)$$

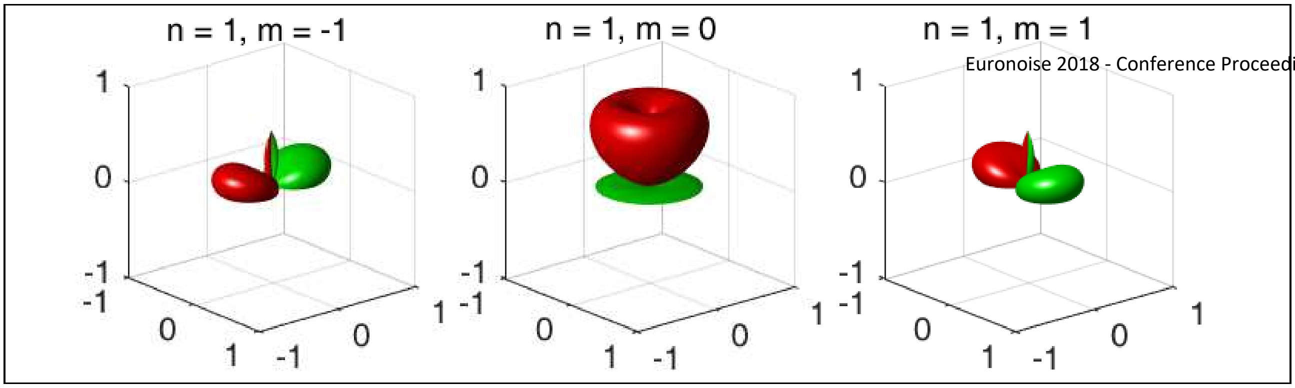

Figure 2: The plot of hemispherical harmonics $H_n^m(\theta,\phi)$, for $n=1, m=-n$ to $+n$. Red denotes the positive regions and green is for negative regions.

2.2. The HSH Basis Function

The orthogonality of $P_n^m(x)$ is over [-1,1] as indicated in (6). The range [-1,1] is due to the fact that the elevation angle θ, in $P_n^m(\cos\theta)$ takes value in $[0,\pi]$. As the paper deals with HMA, the elevation of the sensor must lie in [0,$\pi/2$] or equivalently, $x \in [0,1]$. Hence, a new set of orthogonal associated Legndre polynomials is required. This is achieved by shifting the associated legendre polynomials. In general, if the polynomials $P_{nm}(x)$ are orthogonal over $[a,b]$, with $w(x)$ as a weighting function, then the polynomials $P_{nm}(q_1x+q_2)$ where $q_1 \neq 0$ are orthogonal over an interval $[\frac{a-q_2}{q_1}, \frac{b-q_2}{q_1}]$ with $w(q_1x+q_2)$ as a weighting function [23]. The linear transformation of x to $2x-1$ in (6) gives the shifted ALPs expressed as

$$\tilde{P}_n^m(x) = P_n^m(2x-1). \tag{8}$$

The shifted ALPs are orthogonal over $[0,1]$ with weight function as 1. The orthogonal relation is now expressed as

$$\int_0^1 \tilde{P}_n^m(x)\tilde{P}_{n'}^m(x)dx = \int_0^1 P_n^m(2x-1)P_{n'}^m(2x-1)dx = \frac{(n+m)!}{(2n+1)(n-m)!}\delta_{nn'}. \tag{9}$$

Just as ALPs are used to construct SH basis functions, shifted ALPs are utilized herein to construct a HSH basis functions. The real valued hemispherical harmonics basis functions $H_n^m(\theta,\phi)$ can now be expressed as

$$H_n^m(\theta,\phi) = \begin{cases} (-1)^{|m|}\sqrt{2}\tilde{K}_n^m \sin(|m|\phi)\tilde{P}_n^{|m|}(\cos\theta) & : m<0 \\ (-1)^{|m|}\sqrt{2}\tilde{K}_n^m \cos(m\phi)\tilde{P}_n^{m}(\cos\theta) & : m>0 \\ \tilde{K}_n^0\tilde{P}_n^0(\cos\theta) & : m=0 \end{cases} \tag{10}$$

where $\tilde{K}_n^m$ is the normalization value expressed as

$$\tilde{K}_n^m = \sqrt{\frac{(2n+1)(n-\mid m\mid)!}{2\pi(n+\mid m\mid)!}}. \tag{11}$$

The normalization value maintains the orthogonality of HSH functions, $H_n^m(\theta,\phi)$ over $[0,\pi/2]\times[0,2\pi]$. 3-D plots for HSH functions are given in Figure 2 for $n=1$ and m varying in [-1,1].

3. The Hemispherical Array Data Model

The sound pressure at I microphones, $\mathbf{p}(t) = [p_1(t), p_2(t), ..., p_I(t)]^T$ in spatio-temporal domain can be written as [10]

$$\mathbf{p}(t) = \mathbf{A}(k)\mathbf{s}(t) + \mathbf{n}(t), \tag{12}$$

where $t=1,2,...,N_s$, with N_s being the total snapshots, $\mathbf{s}$ is $L\times N_s$ signal matrix and n is $I\times N_s$ matrix of uncorrelated sensor noise. $A(k)$ is $I\times L$ steering matrix given by

$$\mathbf{A}(k) = \left[\mathbf{a_1}(k_1)\ \mathbf{a_2}(k_2)\ \ldots\ \mathbf{a_L}(k_L)\right]. \tag{13}$$

A particular steering vector can be expressed as

$$\mathbf{a_l}(k_l) = \left[e^{-j\mathbf{k}_l^T\mathbf{r}_1},\ e^{-j\mathbf{k}_l^T\mathbf{r}_2},\ \ldots,e^{-j\mathbf{k}_l^T\mathbf{r}_I}\right]^T, \tag{14}$$

where $\mathbf{k_l}$ is the wave-vector corresponding to the lth plane wave, given by

$$\mathbf{k_l} = -\left[k\sin\theta_l\cos\phi_l,\ k\sin\theta_l\sin\phi_l,\ k\cos\theta_l\right]^T, \tag{15}$$

$\mathbf{r_i}$ is the position vector of ith microphone expressed as

$$\mathbf{r_i} = \left[r\sin\theta_i\cos\phi_i,\ r\sin\theta_i\sin\phi_i,\ r\cos\theta_i\right]^T, \tag{16}$$

$j=\sqrt{-1}$ and $[\ .\ ]^T$ denotes the transpose operator. The ith term in (14) refers to pressure at location r_i due to lth unit amplitude plane wave. This can alternatively be written in spherical coordinate for HMA as

$$e^{-j\mathbf{k}_l^T\mathbf{r}_i} = \sum_{n=0}^{N}\sum_{m=-n}^{n} b_n(kr)H_n^m(\theta_l,\phi_l)H_n^m(\theta_i,\phi_i), \tag{17}$$

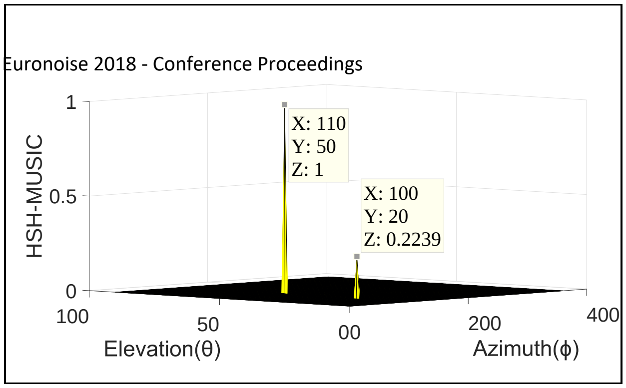

Figure 3: Source localization using HSH-MUSIC. Two sources are at $(20°, 100°)$ and $(50°, 110°)$ with SNR 15 dB.

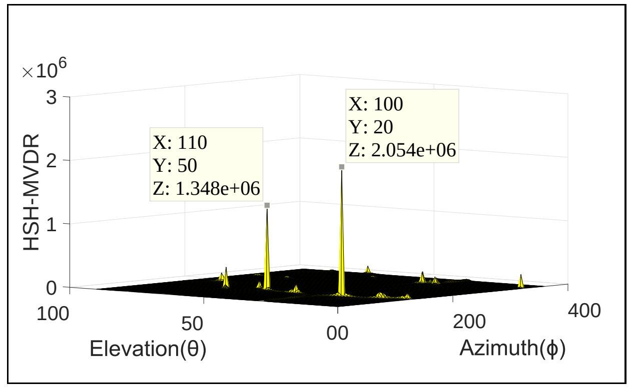

Figure 4: Source localization using HSH-MVDR. Two sources are at $(20°, 100°)$ and $(50°, 110°)$ with SNR 15 dB.

where the finite order N is chosen based on $kr < N \leq \sqrt{I} - 1$ [5]. $b_n(kr)$ is far-field mode strength given by

$$b_n(kr) = \begin{cases} 4\pi j^n (j_n(kr) - \dfrac{j_n^{'}(kr)}{h_n^{'}(kr)}) & : \text{rigid hemisphere} \\ 4\pi j^n j_n(kr) & : \text{open hemisphere} \end{cases} \tag{18}$$

Here, $j_n(kr)$ is the spherical bessel function of first kind. $h_n(kr)$ is spherical Hankel function of second kind and $'$ refers to first derivative. Utilizing (14) and (17) in (13), the steering matrix can be expressed as

$$\mathbf{A}(k) = \mathbf{H}(\Phi)\mathbf{B}(kr)\mathbf{H}^T(\Psi), \tag{19}$$

where $\mathbf{H}(\Phi)$ is a $I \times (N+1)^2$ matrix, whose ith row is defined as

$$h(\Phi_i) = \left[H_0^0(\Phi_i),\ H_1^{-1}(\Phi_i),\ H_1^0(\Phi_i), \dots,\ H_N^N(\Phi_i)\right]. \tag{20}$$

$\mathbf{H}(\Psi)$ is a $L \times (N+1)^2$ matrix whose element can be defined by replacing Φ_i with Ψ_l in (20). $\mathbf{B}(kr)$ is $(N+1)^2 \times (N+1)^2$ matrix given as

$$\mathbf{B}(kr) = \text{diag}\left\{b_0(kr),\ b_1(kr),\ b_1(kr),\ b_1(kr),\ \dots,\ b_n(kr)\right\}. \tag{21}$$

The hemispherical harmonics decomposition of pressure $\mathbf{p}(t)$, received at HMA is given by

$$\begin{aligned} p_{nm}(t,r) &= \int_0^{\pi/2}\int_0^{2\pi} p(t,r,\theta,\phi)[H_n^m(\theta,\phi)]\sin(\theta)d\theta d\phi \\ &\cong \sum_{i=1}^{I} a_i p_i(t,r,\Phi_i)[H_n^m(\Phi_i)], \end{aligned} \tag{22}$$

where a_i is sampling weight of ith microphone [22]. For all $n \in [0, N]$ and $m \in [-n, n]$, (22) can be rewritten in a matrix form as

$$\mathbf{p_{nm}}(t,r) = \mathbf{H^T}(\Phi)\mathbf{\Gamma}\mathbf{p}(t,r,\Phi), \tag{23}$$

where $\mathbf{p_{nm}}(t,r) = \left[p_{00},\ p_{1-1}\ p_{10}\ p_{11}\ \dots\ p_{NN}\right]^T$ and $\mathbf{\Gamma} = diag\left\{a_1,\ a_2,\ a_3,\ \dots a_I\right\}$. The orthogonality of hemispherical harmonics suggests

$$\mathbf{H^T}(\Phi)\mathbf{\Gamma}\mathbf{H}(\Phi) \approx \mathbf{I}, \tag{24}$$

where $\mathbf{I}$ is an identity matrix of dimension $(N+1)^2 \times (N+1)^2$. Substituting (19) in (12), multiplying both side by $\mathbf{H^T}(\Phi)\mathbf{\Gamma}$, utilizing (23),(24) the final data model becomes

$$\mathbf{p_{nm}}(t,r) = \mathbf{B}(kr)\mathbf{H^T}(\Psi)\mathbf{s}(t) + \mathbf{n_{nm}}(t), \tag{25}$$

where $\mathbf{n_{nm}}(t) = \mathbf{H^T}(\Phi)\mathbf{\Gamma}\mathbf{n}(t)$. As the mode strength is constant for a particular array configuration, the final hemispherical harmonics data model can be written as

$$\mathbf{d_{nm}}(t,r) = \mathbf{H^T}(\Psi)\mathbf{s}(t) + \mathbf{z_{nm}}(t), \tag{26}$$

where $\mathbf{z_{nm}}(t) = \mathbf{B}^{-1}(kr)\mathbf{n_{nm}}(t)$ and $\mathbf{d_{nm}}(t,r) = \mathbf{B}^{-1}(kr)\mathbf{p_{nm}}(t,r)$.

4. Acoustic Source Localization using HMA

Having formulated the data model in hemispherical harmonics domain, algorithms for source localization is presented in this Section. In particular, MUSIC and MVDR algorithms are reformulated. Comparing the data model in (12) and (26), the steering matrix in HSH domain is given by $\mathbf{H^T}(\Psi)$.

4.1. The Hemispherical Harmonics MUSIC

The MUSIC spectrum in hemispherical harmonics domain (HSH-MUSIC) can now be written as

$$P_{\text{HSH-MUSIC}}(\Psi) = \frac{1}{h^T(\Psi)\mathbf{Q_{nm}}\mathbf{Q_{nm}}^T h(\Psi)}, \tag{27}$$

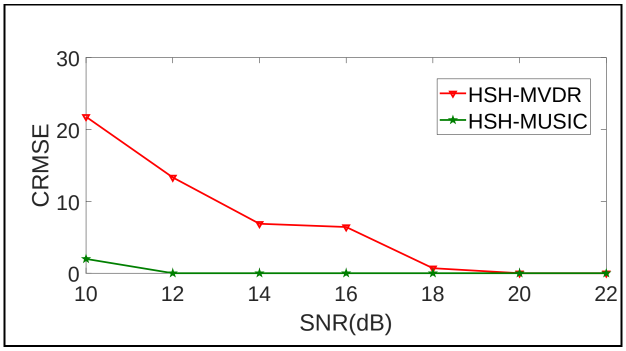

Figure 5: Cumulative RMSE for two sources at $(30°, 100°)$ and $(35°, 110°)$ with various SNRs.

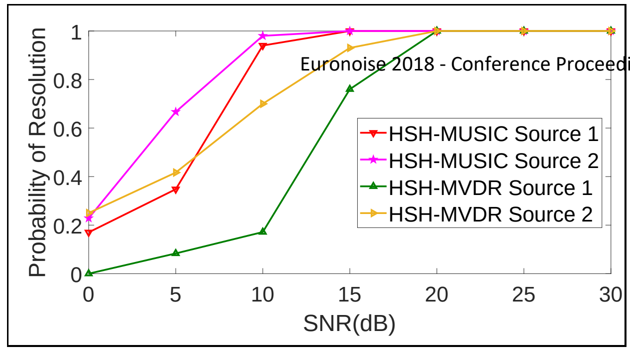

Figure 6: Probability of resolution for two sources at $(30°, 100°)$ and $(35°, 110°)$ with various SNRs.

where $h(\Psi)$ is steering vector defined in (20), $\mathbf{Q_{nm}}$ is noise subspace obtained by eigenvalue decomposition of array covariance matrix, $\mathbf{R_{d_{nm}}}$ given by $\mathbf{R_{d_{nm}}} = E[\mathbf{d_{nm}}(t, r)\mathbf{d_{nm}}(t, r)^T]$. The HSH-MUSIC spectrum gives peak at the location of the sources. This is because, the denominator of the HSH-MUSIC spectrum turns out to be zero when Ψ is the direction of arrival (DOA) owing to the orthogonality between noise eigenvector and steering vector.

4.2. The Hemispherical Harmonics MVDR

MVDR is beamforming based source localization method. The MVDR spectrum in hemispherical harmonics domain (HSH-MVDR) can be formulated as

$$P_{\text{HSH-MVDR}}(\Psi) = \frac{1}{h^T(\Psi)\mathbf{R_{d_{nm}}}^{-1}h(\Psi)}. \tag{28}$$

The MVDR power spectrum gives L peaks corresponding to L sources.

Source localization using HSH-MUSIC and HSH-MVDR is illustrated in Figure 3 and Figure 4 respectively. The simulation is performed considering all the microphones in Eigenmike® system with elevation varying from $0°$ to $90°$. Two sources are taken at $(20°, 100°)$ and $(50°, 110°)$ with 15 dB signal to noise ratio (SNR).

5. Simulation Experiments

Two methods HSH-MUSIC and HSH-MVDR for source localization are proposed herein. A rigid hemisphere of radius 4.2 cm is taken. It consists of all the 20 microphones in Eigenmike® [24] system having elevation from $0°$ to $90°$. The order of the array is taken to be $N = 3$. Root mean square error (RMSE) and probability of resolution measures are used to evaluate performance of the proposed methods. Two sources located at $(30°, 100°)$ and $(35°, 110°)$ are considered. The noise assumed is additive in nature with zero mean Gaussian distribution and unit variance.

5.1. The Cumulative RMSE analysis

The source localization performance is presented herein as cumulative RMSE (CRMSE) formulated as

$$CRMSE_{\theta,\phi} = \frac{1}{4T}\sum_{t=1}^{T}\sum_{l=1}^{2}\left[\theta_l - \tilde{\theta}_{l(t)}\right]^2 + \left[\phi_l - \tilde{\phi}_{l(t)}\right]^2, \tag{29}$$

where t is the trial index, l is the source index, (θ_l, ϕ_l) is the true position of the source and $(\tilde{\theta}_l, \tilde{\phi}_l)$ is the estimated source position. The CRMSE is plotted here for 100 independent Monte Carlo trials. Figure 5 shows the CRMSE plot for the proposed HSH-MUSIC and HSH-MVDR methods at various SNRs. It is to note that the subspace based HSH-MUSIC method has lower CRMSE.

5.2. Probability of Resolution Analysis

Statistical analysis for the proposed methods is presented here using probability of resolution at various SNRs. A confidence interval of $\zeta = 5°$ is used for computing probability over 50 independent trials. The probability of resolution is given by

$$\begin{aligned} P_d = & \frac{1}{2T}\sum_{t=1}^{T}\sum_{l=1}^{2} P_r\left(\left(\left|\theta_l - \tilde{\theta}_{l(t)}\right| \le \zeta\right)\right. \\ & \left.\bigcap\left(\left|\phi_l - \tilde{\phi}_{l(t)}\right| \le \zeta\right)\right), \\ = & \frac{1}{2T}\sum_{t=1}^{T}\sum_{l=1}^{2}\left[sgn\left(\zeta - \left|\theta_l - \tilde{\theta}_{l(t)}\right|\right)\right] \\ & \times\left[sgn\left(\zeta - \left|\phi_l - \tilde{\phi}_{l(t)}\right|\right)\right], \end{aligned} \tag{30}$$

where P_r is the probability of an event and $sgn(x)$ is given by

$$sgn(x) = \begin{cases} 1 & \text{if } x \ge 0, \\ 0 & \text{if } x < 0. \end{cases}$$

The P_d values for HSH-MUSIC and HSH-MVDR are plotted in Figure 6 for various SNRs. It is clear that probability of resolution increases with increasing SNR. Additionally, the subspace based HSH-MUSIC has higher resolving power.

6. Conclusions and Future Work

Far-field source localization using hemispherical microphone array is addressed for the first time in this paper. Hemispherical harmonics basis functions are utilized to formulate MUSIC and MVDR algorithms for source localization. The proposed methods are evaluated using various experiments on source localization. CRMSE and probability of resolution measures are utilized for this. A fast, time domain beamforming algorithm will be worked out in future for capturing and reproducing 3D audio using HMA. Building an own prototype HMA for sound source localization and sound field analysis is also in the future agenda.

References

[1] A. H. Moore, C. Evers, and P. A. Naylor: Direction of arrival estimation in the spherical harmonic domain using subspace pseudo intensity vectors. IEEE/ACM Transactions on Audio, Speech, and Language Processing, 25(1):178-192, Jan. 2017.

[2] P. Samarasinghe, T. D. Abhayapala, and W. Kellermann: Acoustic reciprocity: An extension to spherical harmonics domain. The Journal of the Acoustical Society of America, 142(4):EL337-EL343, Oct. 2017.

[3] L. Kumar and R. M. Hegde: Near-field acoustic source localization and beamforming in spherical harmonics domain. IEEE Transactions on Signal Processing, 64(13):3351-3361, Jul. 2016.

[4] O. Nadiri and B. Rafaely: Localization of multiple speakers under high reverberation using a spherical microphone array and the direct-path dominance test. Transactions on Audio, Speech, and Language Processing, 22(10):1494-1505. Oct. 2014.

[5] J. Meyer and G. Elko: A highly scalable spherical microphone array based on an orthonormal decomposition of the soundfield. In IEEE International Conference on Acoustics, Speech, and Signal Processing, pages II-1781-II-1784, May 2002.

[6] I. Cohen, J. Benesty, and S. Gannot: Speech processing in modern communication: Challenges and perspectives. Springer Science and Business Media, New York, NY, USA, 2010.

[7] D. Khaykin and B. Rafaely: Acoustic analysis by spherical microphone array processing of room impulse responses. The Journal of the Acoustical Society of America, 132(1):261-270, Jul. 2012.

[8] R. Schmidt: Multiple emitter location and signal parameter estimation. IEEE Transactions on Antennas and Propagation, 34(3):276-280, Mar. 1986.

[9] X. Li, S. Yan, X. Ma, and C. Hou: Spherical harmonics MUSIC versus conventional MUSIC. Applied Acoustics, 72(9):646-652, Sep. 2011.

[10] R. Roy and T. Kailath: ESPRIT-estimation of signal parameters via rotational invariance techniques. IEEE Transactions on Audio, Speech, and Language Processing, 37(7):984-995, Jul. 1989.

[11] R. Goossens and H. Rogier: Closed-form 2D angle estimation with a spherical array via spherical phase mode excitation and ESPRIT. In IEEE International Conference on Acoustics, Speech and Signal Processing, pages 2321-2324, Mar. 2008.

[12] H. Sun, H. Teutsch, E. Mabande, and W. Kellermann: Robust localization of multiple sources in reverberant environments using EB-ESPRIT with spherical microphone arrays. In IEEE International Conference on Acoustics, Speech and Signal Processing, pages 117-120, May 2011.

[13] L. Kumar, G. Bi, and R. M. Hegde: The spherical harmonics root-MUSIC. In IEEE International Conference on Acoustics, Speech and Signal Processing, pages 3046-3050, Mar. 2016.

[14] Z. Li and R. Ruraiswami: Hemispherical microphone arrays for sound capture and beamforming. In IEEE Workshop on Applications of Signal Processing to Audio and Acoustics, pages 106-109, Oct. 2005.

[15] B. Cabral, N. Max, and R. Springmeyer: Bidirectional reflection functions from surface bump maps. In 14th Annual Conference on Computer Graphics and Interactive Techniques, pages 273-281, Jul. 1987.

[16] P.-P. Sloan, J. Kautz, and J. Snyder: Precomputed radiance transfer for real-time rendering in dynamic, low-frequency lighting environments. ACM Transactions on Graphics, 21(3):527-536, Jul. 2002.

[17] S. H. Westin, J. R. Arvo, and K. E. Torrance: Predicting reflectance functions from complex surfaces, In 19th Annual Conference on Computer Graphics and Interactive Techniques, pages 255-264, Jul. 1992.

[18] P. Gautron, J. Krivanek, S. N. Pattanaik, and K. Bouatouch: A novel hemispherical basis for accurate and efficient rendering. In 15th Eurographics Conference on Rendering Techniques, pages 321-330, Jun. 2004.

[19] P. N. Samarasinghe and T. D. Abhayapala: Blind estimation of directional properties of room reverberation using a spherical microphone array. In IEEE International Conference on Acoustics, Speech and Signal Processing, pages 351-355, Mar. 2017.

[20] H. Huang, L. Zhang, D. Samaras, L. Shen, R. Zhang, F. Makedon, and J. Pearlman: Hemispherical harmonic surface description and applications to medical image analysis. In Third International Symposium on 3D Data Processing, Visualization and Transmission, pages 381-388, Jun. 2006.

[21] D. P. Jarrett, E. A. P. Habets, and P. A. Naylor: Theory and applications of spherical microphone array processing. Springer, Berlin, Germany, 2017.

[22] B. Rafaely: Analysis and design of spherical microphone arrays. IEEE Transactions on Speech and Audio Processing, 13(1):135-143, Jan. 2005.

[23] G. Szegö: Orthogonal polynomials, 4 ed. American Mathematical Society, Providence, Rhode Island, USA 1975.

[24] The Eigenmike Microphone Array, http://www.mhacoustics.com/.